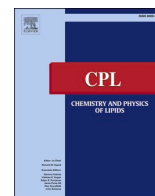# Ionizable lipids penetrate phospholipid bilayers with high phase transition temperatures: perspectives from free energy calculations

(article starts on next page)

Research paper

Ionizable lipids penetrate phospholipid bilayers with high phase transition temperatures: perspectives from free energy calculations

Inna Ermilova [*], Jan Swenson

Department of Physics, Chalmers Uiversity of Technology, SE 412 96 Gothenburg, Sweden

ABSTRACT

The efficacies of modern gene-therapies strongly depend on their contents. At the same time the most potent formulations might not contain the best compounds. In this work we investigated the effect of phospholipids and their saturation on the binding ability of (6Z,9Z,28Z,31Z)-heptatriacont-6,9,28,31-tetraene-19-yl 4-(dimethylamino) butanoate (DLin-MC3-DMA) to model membranes at the neutral pH. We discovered that DLin-MC3-DMA has affinity to the most saturated monocomponent lipid bilayer 1,2-dimyristoyl-*sn*-glycero-3-phosphocholine (DMPC) and an aversion to the unsaturated one 1,2-dioleoyl-*sn*-glycero-3-phosphocholine (DOPC). The preference to a certain membrane was also well-correlated to the phase transition temperatures of phospholipid bilayers, and to their structural and dynamical properties. Additionally, in the case of the presence of DLin-MC3-DMA in the membrane with DOPC the ionizable lipid penetrated it, which indicates possible synergistic effects. Comparisons with other ionizable lipids were performed using a model lipid bilayer of 1-palmitoyl-2-oleoyl-glycero-3-phosphocholine (POPC). Particularly, the lipids heptadecan-9-yl 8-[2-hydroxyethyl-(6-oxo-6-undecoxyhexyl)amino]octanoate (SM-102) and [(4-hydroxybutyl) azanediyl] di(hexane-6,1-diyl) bis(2-hexyldecanoate) (ALC-0315) from modern mRNA-vaccines against COVID-19 were investigated and force fields parameters were derived for those new lipids. It was discovered that ALC-0315 binds strongest to the membrane, while DLin-MC3-DMA is not able to reside in the bilayer center. The ability to penetrate the membrane POPC by SM-102 and ALC-0315 can be related to their saturation, comparing to DLin-MC3-DMA.

1. Introduction

Growing numbers of outbreaks of various diseases such as COVID-19 Niu and Xu (2020), monkeypox Venkatesan (2022), polio Awan et al. (2022) and many others (Ward et al.; Makoni, 2022; Okonji et al., 2022) gave a kick-start to usage of mRNA gene-therapies as vaccines against them Verbeke et al. (2021). These vaccines are also seen as potential treatments against cardiovascular diseases (Hadas et al., 2019; Rabinovich et al., 2006), Alzheimer's disease (Grabowska-Pyrzewicz et al., 2021; Lei et al., 2020), cancer (Wang et al., 2022; Pascolo, 2008) etc.

Formulations of mRNA-containing lipid nanoparticles (LNPs) are usually including such compounds as phospholipids, cholesterol, mRNA and its stabilizers, salt and ionizable lipids (Patel et al., 2022; Yanez Arteta et al., 2018; Albertsen et al., 2022). The efficacy of these LNPs depends on the ratios between the mixed components as well as on their individual physical, chemical and structural properties.

Structures of the LNPs were never precisely determined for many reasons. Experimental techniques can mainly provide data about average shapes and sizes of LNPs (Brader et al., 2021; Yanez Arteta et al., 2018), but not about the important internal structure of LNPs. Furthermore, their sizes and complexity can be impossible to handle by any refinement program on atomistic level due to limitations by both software and hardware. A polydispersity of such systems implies that particles of different sizes can have discrepant compositions (Yanez Arteta et al., 2018; Kon et al., 2022; Malburet et al., 2022). Structural instability of mRNA (Kon et al., 2022; Yanez Arteta et al., 2018; Sebastiani et al., 2021; Cui et al., 2022) can be a cause of polydispersity of LNPs, which makes it more challenging for determining the exact locations of compounds in nanoparticles by scattering techniques. However, a generalized idea about the contents of various parts of LNPs was obtained (Sebastiani et al., 2021; Schoenmaker et al., 2021; Viger-Gravel et al., 2018).

In a recent paper Sebastiani et al. (2021) managed to describe compounds in the core and shell of LNPs containing DLin-MC3-DMA out of small-angle neutron scattering data by mentioning their amounts in the respective parts of LNPs. Particularly, all lipid components were

present in the shell. Nevertheless, their data did not suggest the exact distribution of ingredients because of the complex composition and structure. According to even earlier works with scattering techniques, Heberle et al. (2013) the structural complexity was even observed in simpler systems like lipid vesicles, where only phospholipids were present in mixtures. Various domain formations were observed in the shells of those vesicles. Viger-Gravel et al. (2018) studied LNPs with siRNA and mRNA using nuclear magnetic resonance spectroscopy and proposed approximate structures of the nanoparticles, but did not deliver any detailed structure on an atomistic level.

Moreover, proposed approximate models for LNPs can only be used for particular components and their ratios, and not be considered as universal models for all mixtures. For example, the presence of a different phospholipid can change the transfection properties according to Kulkarni et al. (2019). Furthermore, Sayers et al. (2019) mentioned that the efficacy of LNPs depends on the properties of the targeted cells. This means that the same formulation will not be appropriate for all applications.

The fact that phospholipids are present in both LNPs and target cells (Söderberg et al., 1990; Sahu and Lynn, 1977; Szlasa et al., 2020) makes it interesting to investigate possible interactions between them and ionizable lipids from a thermodynamic point of view, using molecular simulations. Finding reasons for the ability of a certain ionizable lipid to penetrate a selected lipid bilayer can help to understand possible reasons behind good transfection properties of LNPs and their toxicity (Kulkarni et al., 2017; Munson et al., 2021; Ndeupen et al., 2021).

Such a study can be performed using a smaller model membrane and employing parallel tempered metadynamics simulations for free energy calculations (Golla et al., 2020; Pokhrel and Maibaum, 2018; Abrams and Bussi, 2013; Ermilova and Lyubartsev, 2020). The reason why a thermodynamic approach can be considered as the most appropriate here is because in classical molecular dynamics (MD) simulations the short time scale might not be enough to see a phenomenon happening. For instance, in a real life a penetration of a large molecule through a membrane might take hours while in atomistic MD simulations the time scale might go to microseconds (Walter and Gutknecht, 1986; Kucherak et al., 2010; Gu et al., 2019).

Earlier we have carried out a comparative study of the behavior of the neutral form of DLin-MC3-DMA in phospholipid bilayers containing DOPC (18:1–18:1 PC) and DOPE (18:1–18:1 PE) lipids at two ratios of the ionizable lipids Ermilova and Swenson (2020). We have seen that DLin-MC3-DMA could be present inside the bilayers as well as at their surfaces. In another work by Park et al. (2021), where the more saturated lipids POPC (16:0–18:1 PC) and POPE (16:0–18:1 PE) were used, DLin-MC3-DMA was observed in larger amounts in the bilayer center. This could be caused by phospholipid saturation, different

concentrations as well as by a different starting geometry of a bilayer. For instance, if an algorithm places ionizable lipids too close to each other in the starting configuration, it can result in their aggregation in the beginning of simulation. Therefore, understanding the role of lipid tail saturation on interactions between phosphatidylcholines and ionizable lipids is a very important task, because it would unveil its role on transfection properties and possible toxicity of LNPs and help to optimize them.

In this work, interactions between most prominent ionizable lipids (ALC-0315, SM-103 and DLin-MC-DMA) and phospholipids (see Fig. 1) at neutral pH are investigated by free energy calculations. The goal is to understand if any of the studied compounds could penetrate the membrane at such a pH as well as to find out how the saturation of phospholipids could affect this process. These ionizable lipids were chosen since DLin-MC3-DMA is considered as the most prominent compound Jayaraman et al. (2012), but SM-102 and ALC-0315 became the ingredients of approved mRNA-vaccines against COVID-19 (Xia, 2021; Suzuki and Ishihara, 2021) by Moderna and Pfizer respectively. Model lipid bilayer membranes containing DMPC, POPC, 1-stearoyl-2-oleoyl-*sn*-glycero-3-phosphocholine (SOPC) and DOPC were selected due to their phase behavior at 298 K, which can simplify free energy calculations. At last but not least, we would like to see what kind of correlation there is between experimental physical properties of the studied lipid bilayers and computed binding free energies.

2. Method

2.1. Parametrization of lipid models

Models for ALC-0315 and SM-102 were derived by applying the same philosophy and methodology as was done in the case of polyunsaturated phospholipids and DLin-MC3-DMA adopted from the SLipids force field (FF) (Jämbeck and Lyubartsev, 2012,2013; Ermilova and Lyubartsev, 2016; Ermilova and Swenson, 2020).

The general form of the SLipids FF can be written as:

$$E_{FF} = E_{bonded} + E_{non-bonded}, \tag{1}$$

where:

$$E_{bonded} = E_{angles} + E_{dihedrals} + E_{bonds} + E_{Urey-Bradley} \tag{2}$$

and:

$$E_{non-bonded} = E_{Lennard-Jones} + E_{Coulumb}. \tag{3}$$

Since all parameters for bonds, angles and dihedrals can be obtained from earlier versions of the SLipids FF, in this work only partial atomic charges are derived, which can be easily added to the FF using the
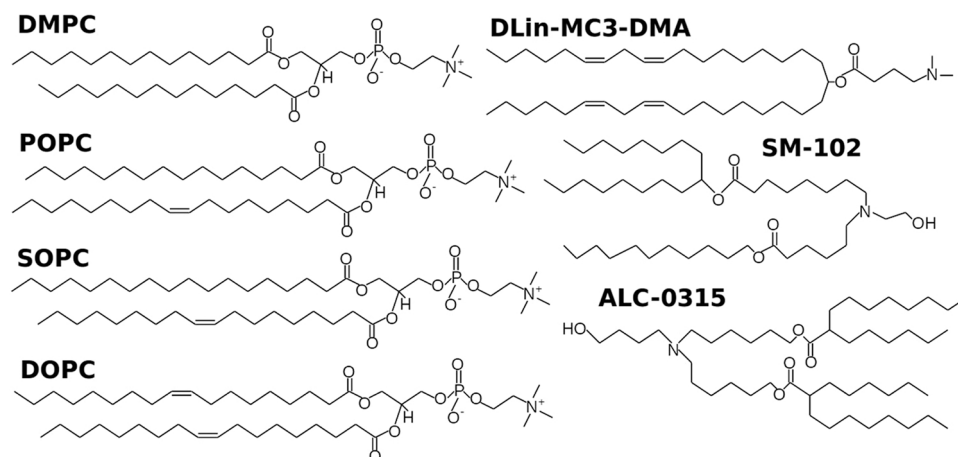

Fig. 1. Lipids used in the simulations.

following equation (4):

$$E_{Coulomb} = \sum_{i,j} \frac{q_i q_j}{4\pi\varepsilon_0 r_{i,j}} \qquad (4)$$

Moreover, due to the availability of more efficient hardware it was possible to compute them without dividing large lipid molecules into small ones, as it was done in earlier versions of SLipids FF. 50 random conformations were created for every lipid. Then the computations of partial atomic charges were carried out using the B3LYP (Becke, 1993; Lee et al., 1988; Stephens et al., 1994) level of theory with the basis set cc-pVTZ Kendall et al. (1992) in *Gaussian*09 software Frisch et al. (2009) together with the restrained electrostatic potential approach (RESP) Cornell et al. (2002) in the R.E.D. software Dupradeau et al. (2010). The whole lipids were placed firstly in a polarizable continuum with a dielectric constant of 78.4 in the IEFPCM model (Tomasi et al., 1999; Pomelli et al., 2001) in order to mimic the solvent effects and their induced polarization on the charge distribution. In order to take into consideration hydrophobic effects, calculations for the same set of configurations were performed using a solvent model with a dielectric constant of 2.04. This appears to be a reasonable approach because from our previous paper Ermilova and Swenson (2020) as well as from a number of experimental studies it follows that ionizable lipids do not have preferential orientations (not bilayer building lipids) like phosphatidylcholines (Jayaraman et al., 2012; Kulkarni et al., 2017), which makes it unreasonable to divide those molecules into purely hydrophobic and hydrophilic parts. Then final values were averaged and written to a database following the same ideas of FFs' transferability (Ermilova and Lyubartsev, 2016; Ermilova and Swenson, 2020).

Final models for SM-102 and ALC-0315 can be found in Figures S1-S2 in Supporting Information.

2.2. Binding free energy calculations

Parallel-tempered metadynamics is a useful approach when one wants to study a penetration of larger molecules through lipid bilayers (Barducci et al., 2008; Bonomi et al., 2009; Bussi and Laio, 2020; Ermilova and Swenson, 2020; Pfaendtner, 2019; Bussi et al., 2006). Here a statistics over several parallel simulations is collected and averaged in order to calculate the total potential of mean force (PMF) profile and the actual binding free energy. This approach can give a better sampling over molecular conformations and possible states of the systems. A single simulation here would need to be very long for obtaining good data.

For pure phospholipid bilayers pre-equilibrated membranes were taken from earlier simulations which were downloaded from the SLipids FF web-page: every system contained 128 lipids (64 lipids per 1 leaflet). Thereafter, ionizable lipids were added at a distance of at least 1 *nm* from the membranes' surfaces. 10240 water molecules with the water model TIP3p Jorgensen et al. (1983) were added to every system in order to let the ionizable lipid move freely along the *z*-coordinate. To ensure that none of them would end up in the membrane artificial van der Waals spheres of the radius of 0.5 *nm* were applied around each atom of every lipid. All systems were thereafter pre-equilibrated for about 120 *ns* in NPT ensemble at a pressure of 1 *atm*. and a temperature of 298 *K* using Berendsen barostat with semi-isotropic pressure coupling system Berendsen et al. (1984). The time constant was about 10 *ps* and the isothermal compressibility 0.000045 1/*bar*. Temperature coupling was performed using the Velocity Rescale algorithm with a time constant of 0.5 *ps*Bussi et al. (2007). The integrator was leap-frog with a time step of 2 *fs*. Bonds were constrained using LINCS algorithm with 12 iterations (Hess et al., 1997; Hess, 2008). The cut-off value was 0.9 nm with so-called van der Waals modifier Potential-shift Essmann et al. (1995). Long-range electrostatics were computed using the Particle Mesh Ewald algorithm (PME) Darden et al. (1993) with the order equal to 4. The MD engine was GROMACS-2019 (Berendsen et al., 1995; Hess, 2008).

Bilayers containing various amounts of DLin-MC3-DMA were created in a similar way. One membrane contained 112 DOPC and 16 DLin-MC3-DMA lipids, another one had 106 DOPC and 22 DLin-MC3-DMA lipids. Ionizable lipids were placed randomly so that their clustering could be avoided during the equilibration process. 6400 TIP3p Jorgensen et al. (1983) water molecules were added to every system in order to equilibrate those membranes faster. All the settings for these simulations were exactly the same as the ones described above for pure phospholipid bilayers. Last frames from equilibrated systems were taken without water molecules, i.e. 6400 water molecules were deleted and only equilibrated membranes were kept. Then one molecule of DLin-MC3-DMA was inserted in those resulting simulation boxes at a distance of at least 1 *nm* from each membrane. After the addition of all water (10240 molecules) another equilibration was done exactly in the same way as for systems with pure lipid bilayers. The reason why these membranes were created in the described way is because pure lipid bilayers were equilibrated originally with a smaller water content and without any ionizable lipid in the boxes. Therefore, the pre-equilibration of membranes with 128 lipids is conducted with 6400 water molecules, before adding 1 ionizable lipid and more water. Detailed compositions of simulated systems can be observed in Table S1 in Supporting Information.

The MD part for the free energy calculations were carried out using NVT ensemble with Velocity Rescale thermostat Bussi et al. (2007). NVT ensemble is chosen for accurate calculations of membranes' centers of mass (Ermilova et al., 2017; Ermilova and Lyubartsev, 2019; Martí, 2018; Yang et al., 2016). All other settings for the MD engine were the same as during the equilibration. The code which was employed for parallel-tempered metadynamics was *plumed* − 2.5. 4Tribello et al. (2014). A collective variable selected for biasing the calculation of PMF was the *Z*-component of the distance between centers of mass of a membrane and a chosen ionizable lipid molecule. This collective variable was selected in order to avoid high computational costs which one could face in case of choosing to compute the radius of gyration as well. Then the computation would become two dimensional and would take longer time to converge. Radius of gyration (Lobanov et al., 2008; He and Niemeyer, 2003) is monitored and averaged in the end of every simulation. The threshold of 0.2 nm is chosen as an accepted value in considerations of the accuracy of simulations.

At the same time that selected molecule was kept as the whole for accurate calculations. In every system with DOPC and various amounts of DLin-MC3-DMA only a single molecule of the latter compound was taken into consideration for computations. The bias factor (γ) was equal to 100. The height of each Gaussian function was 1.2 *kJ/mol* and its width (σ) was 0.05 *nm*. Gaussian functions were deposited every 500 steps. For every system with a certain membrane and the ionizable lipid, 5 random starting configurations were created out of equilibrated parts of MD trajectories in order to be able to run the multi-walkers algorithm Deighan et al. (2012). The length of each simulation was 600 *ns*.

3. Results and discussion

3.1. Binding free energies

Before computing the potential of mean force profiles the radius of gyration was calculated for single lipids which were used for biasing in free energy simulations (see Section 2 in Supporting Information). Since the radius of gyration is directly related to the molecular geometries, it can help to verify that the conformational differences are not too large and, therefore, the results are comparable and acceptable among all simulated ionizable lipids. Table S2 (obtained out of data in Figures S3-S10 in Supporting Information) shows that values of radius of gyration are very similar for all ionizable lipids, i.e. all average values of the radius of gyration are below 0.15 nm which is even lower than the chosen threshold of 0.2 nm. Furthermore, the free energy calculations are based on the average of all the different conformations of the lipid molecules. These facts lead to the conclusion that the choice of collective

variable is reasonable and results for potential of mean force profiles are comparable and reliable.

Potential of mean force profiles graphically demonstrate in which phase the ionizable lipid prefers to be: in a membrane or in water. A higher value of the potential at a certain coordinate means a lower probability to find the molecule there. Binding free energies are computed from PMF profiles in order to tell more precisely about the affinity of an ionizable lipid to a certain membrane using the formula (5):

$$\Delta G_{bind} = -k_B T ln\left(\frac{\int_B e^{-w(z)k_B T}dz}{\int_U e^{-w(z)k_B T}dz}\right) \qquad (5)$$

Here ΔG_{bind}° is the binding free energy, k_B is the Boltzman's constant, T is the temperature in K, z is the distance in the direction perpendicular to the membrane layer between the centers of mass of the membrane and the ionizable lipid, U and B are "unbounded" (outside of the lipid bilayer, at a distance above 2.5 nm from the bilayer center) and "bounded" (inside the membrane, at a distance below 2.5 nm from the bilayer center) states respectively.

Fig. 2(a) demonstrates profiles for DLin-MC3-DMA in various monocomponent lipid bilayers. The bilayer of DMPC is the most saturated membrane among all and the ionizable lipid can easily enter it and even

to reside in its center. In lipid bilayers of POPC and SOPC DLin-MC3-DMA can enter the membrane but does not reside in its center, which can probably be due to interactions with unsaturated parts of lipid tails. Finally, in the case of DOPC the ionizable lipid remains at the membrane surface. Values from Table 1 confirm the statements above and place the affinity of DLin-MC3-DMA to pure phospholipid bilayers in the following increasing order: DOPC < POPC < SOPC < DMPC.

Comparing DLin-MC3-DMA with SM-102 and ALC-0315 in the presence of the lipid bilayer of POPC (see Fig. 2(b)) it can be concluded that ALC-0315 has the highest affinity to the membrane, while DLin-

Table 1
Binding free energies in kJ/mol (error is within 2 kJ/mol).

System/Molecules	ΔG_{bind}
DMPC, DLin-MC3-DMA	− 29.96
POPC, DLin-MC3-DMA	− 13.87
SOPC, DLin-MC3-DMA	− 19.03
DOPC, DLin-MC3-DMA	− 0.37
POPC, ALC-0315	− 80.72
POPC, SMN-102	− 30.20
DOPC, 12.5%DLin-MC3-DMA	− 43.38
DOPC, 18%DLin-MC3-DMA	− 49.37
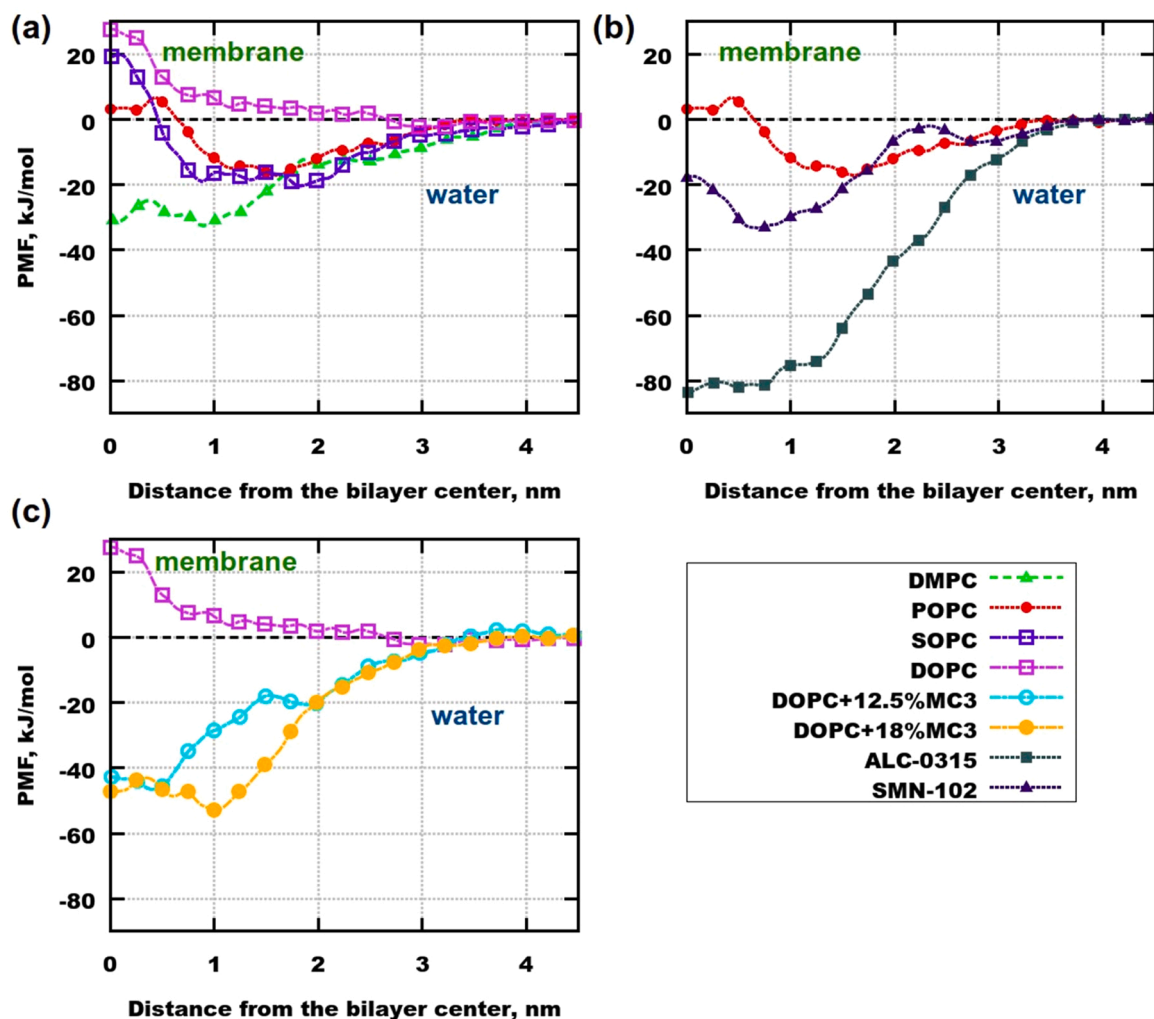
Fig. 2. Potential of mean force profiles (error is within 2 kJ/mol). (a) Simulations with DLin-MC3-DMA in monocomponent bilayers. (b) Simulations with DLin-MC3-DMA, ALC-0315 and SM-102 in POPC. (c) Simulations with DOPC and various amounts of DLin-MC3-DMA. When PMF is close or equal to zero the ionizable lipid is in water, therefore, membrane and water are distinguished. Convergence profiles can be seen in Figs. S11-S18 and profiles for the collective variables are in Figs. S19-S26 in Supporting Information. Convergence profiles can be seen in Figs. S11-S18, profiles for the collective variables are in Figs. S19-S26 and profiles for distances between center of mass of membranes and nitrogen atoms in ionizable lipids on Figures S27-S34 in Supporting Information.

MC3-DMA has the lowest. Both ALC-0315 and SM-102 can easily reside in the center of the lipid bilayer. This is also coherent with the data presented in Table 1.

The affinity of a single molecule of DLin-MC3-DMA to a bilayer which is loaded with some amount of it is shown in Fig. 2(c) for membranes with DOPC. The ionizable lipid is not tending to enter a mono-component bilayer, but it has an affinity to a membrane if there is some quantity of DLin-MC3-DMA, which means that synergistic effects play a role in the binding process (see Table 1).

This finding might rise the question why DLin-MC3-DMA can be present in the lipid bilayer if the ionizable lipid has an aversion to the membrane with only DOPC? The answer is that during the sample preparation of LNPs all lipids are present in the mixture, i.e. DLin-MC3-DMA is not added to any formed lipid bilayers (Sebastiani et al., 2021; Yanez Arteta et al., 2018). Therefore, some quantities of DLin-MC3-DMA can be present in the shell of such LNPs Sebastiani et al. (2021).

3.2. Pure phospholipid bilayers and DLin-MC3-DMA

All properties of materials are strongly dependent on the temperature. This fact is true also for phospholipid bilayers. In their case the properties change dramatically at their phase transition temperatures from gel to liquid phases. In order to find whether there is a strong correlation between physical properties of lipid bilayers and binding free energies of DLin-MC3-DMA the Pearson's correlation coefficient (Benesty et al., 2009; Ermilova et al., 2017) was used, which was calculated according the the following equation (6):

$$\rho_{(X,Y)} = \frac{cov(X, Y)}{\sigma_X \sigma_Y} \tag{6}$$

Where *cov* is a covariance, σ_X is the standard deviation of variable X, σ_Y is the standard deviation of variable Y and $\rho_{(X, Y)}$ is the Pearson's correlation coefficient.

Fig. 3 demonstrates that for a membrane in a liquid phase with a high phase transition temperature Silvius (1982) (a saturated lipid bilayer of DMPC) DLin-MC3-DMA has a higher ability to penetrate such a phospholipid bilayer. This strong relation between the binding free energy and the phase transition temperature is further supported by the Pearson correlation coefficient (Sedgwick, 2012; Ermilova et al., 2017), ρ, equal to -0.994, i.e. an almost perfect inverse relation. It turns out that in case of the most unsaturated phospholipid bilayer, DOPC, with a lower phase transition temperature, it is highly unlikely that an ionizable lipid
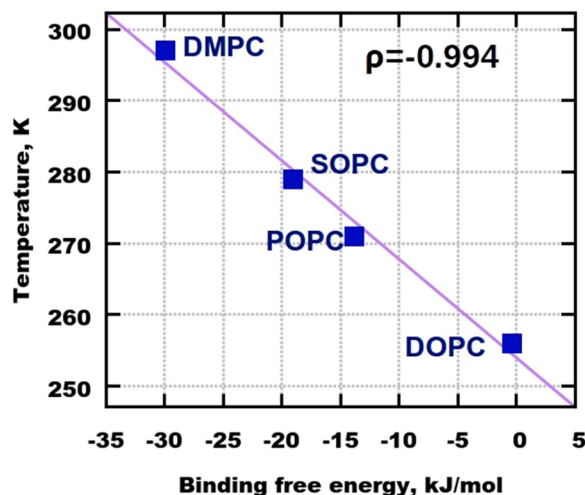
can enter the membrane, but can reside at its surface.

The ability of DLin-MC3-DMA to enter a certain membrane can be also correlated with the area per lipid of the phospholipid building that membrane. Fig. 4(a) shows that with an increasing area per lipid there is a reducing probability that DLin-MC3-DMA will penetrate the membrane. Therefore, the saturated membrane with DMPC Filippov et al. (2007) has the lowest area per lipid and the most unsaturated lipid bilayer with DOPC Tristram-Nagle et al. (1998) has the highest area per lipid. The Pearson correlation coefficient is equal to 0.967 in this case.

Lateral diffusion is also a temperature dependent parameter which can play a role on the ability of a molecule to penetrate a lipid bilayer. Fig. 4(b) shows lateral diffusion coefficients for pure phospholipid bilayers plotted versus the binding free energy of DLin-MC3-DMA. According to the presented data and the Pearson correlation coefficient equal to 0.950, fast planar motions of lipids can prevent ionizable lipids from passing through the membrane.

Since a strong correlation between phospholipid tail saturation and binding free energy of DLin-MC3-DMA was confirmed, there could also be a relation between the elastic properties of the simulated membranes and the binding free energies of the ionizable lipids. For instance, a tilt modulus which is related to the stretching of hydrocarbon chains can be a possible indicator here (Nagle, 2017; May et al., 2004; Jablin et al., 2014). Fig. 5(a) demonstrates such a correlation between binding free energies of DLin-MC3-DMA and experimental tilt modulus Nagle (2017) of simulated membranes. The binding free energy increases with an increasing value of the tilt modulus, and the Pearson correlation coefficient is equal to 0.992, which means that the actual ability to penetrate the membrane decreases with an increasing value of the modulus. Despite that experimental values were obtained at the temperature of 303 K conclusions could be considered as accurate ones, because all lipid bilayers were in the liquid phase.

Another interesting characteristic of a membrane is the relationship between tilt dependent (K_C^{td}) and tilt independent (K_C^{ti}) bending modulus (Chu et al., 2005; Nagle, 2017; Nagle et al., 2015) which can provide thermodynamic information about the elasticity of lipid bilayers during an increased corrugation. Fig. 5(b) shows that when the value of K_C^{ti}/K_C^{td} decreases the binding free energy increases (the Pearson correlation coefficient is -0.952), which means that DLin-MC3-DMA has a weaker affinity to membranes with lower values of K_C^{ti}/K_C^{td}, like in the case of bilayer with DOPC.

Finalizing the discussion for DLin-MC3-DMA in simulations with four monocomponent phospholipd bilayers it can be concluded that the ionizable lipid has a stronger affinity to more saturated membranes, such as of DMPC, when they are in the liquid phase. Moreover, when entering partially unsaturated membranes, like the ones with POPC and SOPC, interactions with unsaturated lipid tails might prevent DLin-MC3-DMA from penetrating them.

3.3. DOPC and DLin-MC3-DMA: synergistic effects

Since the binding free energy for DLin-MC3-DMA in membranes containing pure DOPC was higher than for lipid bilayers with DOPC loaded with the same ionizable lipid, it can be reasonable to think about synergistic effects. They can be caused by some amounts of DLin-MC3-DMA residing at the membrane surface as well as inside the bilayer itself. Such an effect was described earlier in a paper by Ermilova and Swenson (2020).

Fig. 6 shows snapshots of simulated systems containing membranes with pure DOPC and DOPC with some amounts of DLin-MC3-DMA. From the visual observation it can be concluded that lipid bilayers containing some ionizable lipids are appearing to be more deformed. DLin-MC3-DMA molecules can be detected at both the surface and in the bilayer center.

In order to understand more quantitative effects of the ionizable lipids on their ability to penetrate the membranes partial mass density
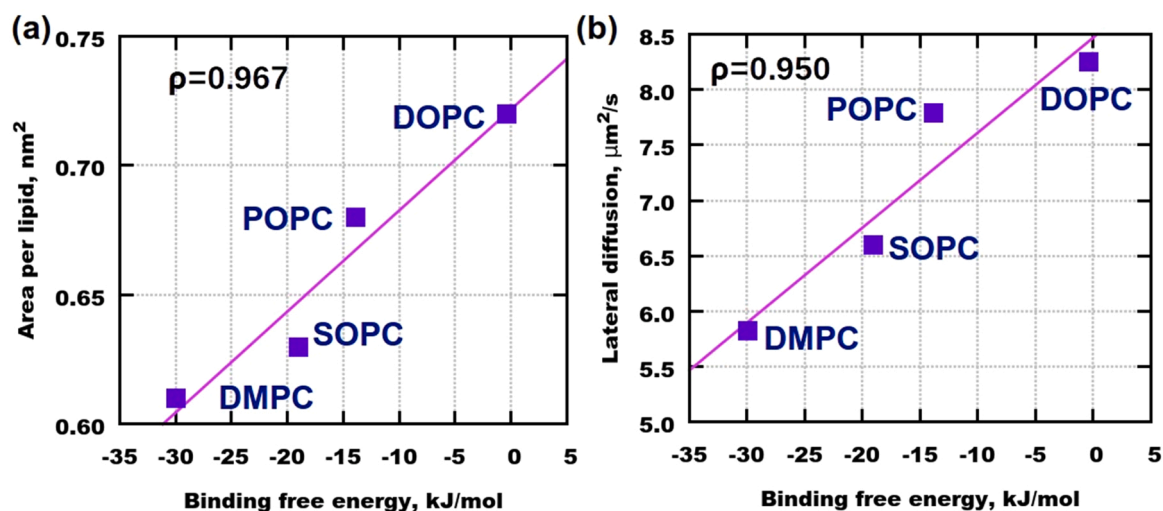

Fig. 3. Phase transition temperatures (Silvius, 1982,1991) of pure phospholipid bilayers versus computed binding free energies of DLin-MC3-DMA. ρ is Pearson correlation coefficient. Errors in binding free energies are within 2 kJ/mol while in temperatures can be seen in references, mentioned above.

Fig. 4. Experimental areas (Tristram-Nagle et al., 1998; Filippov et al., 2007; Lindblom and Orädd, 2009) per lipid (a) and lateral diffusion coefficients (Filippov et al., 2003; Orädd et al., 2002; Filippov et al., 2007; Lindblom and Orädd, 2009) (b) of pure phospholipid bilayers at 298 K versus computed binding free energies of DLin-MC3-DMA. ρ is Pearson correlation coefficient. Errors in binding free energies are within 2 kJ/mol while in temperatures can be seen in references, mentioned above.

Fig. 5. Experimental Nagle (2017) tilt modulus (a) and a relationship between tilt dependent (K_C^{td}) and tilt independent (K_C^{ti}) bending modulus (b) at 303 K versus computed binding free energies of DLin-MC3-DMA. ρ is Pearson correlation coefficient. Errors in binding free energies are within 2 kJ/mol while in temperatures can be seen in references, mentioned above.
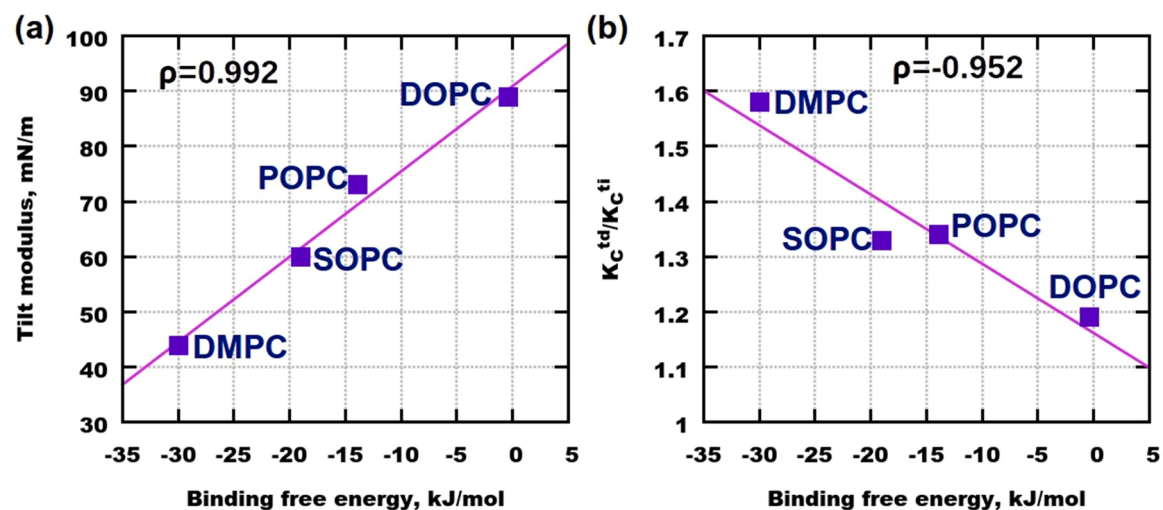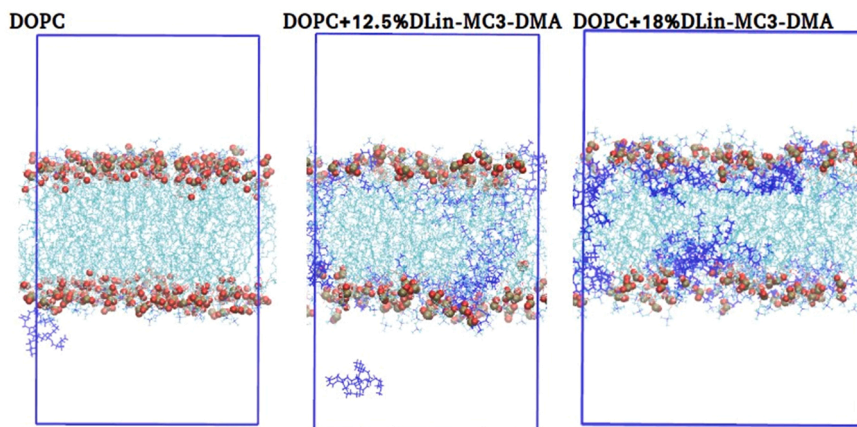

Fig. 6. Snapshots of lipid bilayers. Water molecules are omitted for the clarity. Dark blue molecules are DLin-MC3-DMA. Lipid tails of DOPC are in bright cyan colour. Red and dark yellow spheres at the surface of the membrane are phosphatic groups of phospholipids.

profiles were calculated together with PMF profiles. Fig. 7(a) shows that the highest value of PMF is associated with the location of double bonds of DOPC lipids.

When some DLin-MC3-DMA is present in the membrane the barrier disappears in PMF, as it can be observed in Fig. 7(b)-(c). This also coincides with the fact that some quantities of DLin-MC3-DMA are located around the phosphatic groups, which probably contributes to the lower energy of entering the membrane comparing to the lipid bilayer containing pure DOPC. These results are coherent with findings presented in our previous work Ermilova and Swenson (2020) regarding synergistic effects which occur in phospholipid bilayers loaded with DLin-MC3-DMA.

### 3.4. Comparison of DLin-MC3-DMA, SM-102 and ALC-0315

Two other ionizable lipids of interest are SM-102 and ALC-0315 due to their use in modern mRNA-vaccines against COVID-19. Are these lipids behaving similar to DLin-MC3-DMA or not? There are not enough experimental studies with ionizable lipids in databases which could help to answer this question. However, experimental acid dissociation constant (pK_a) (Hassett et al., 2019; Suzuki and Ishihara, 2021; Ansell and Du, 2015) values have been reported for all three lipids (see Table 2), but one can probably correlate them with binding free energies only for saturated SM-102 and ALC-0315, because in the case of DLin-MC3-DMA unsaturated lipid tails can affect its ability to penetrate model

membranes if those ones also contain unsaturated parts, as in the case of POPC. *clogP*Eygeris et al. (2021) values are showing the logarithm of compound's partition coefficient between *n*-octanol and water. In the same table it can be observed that the highest value of it is for DLin-MC3-DMA, while the lowest one is for SM-102. This suggests that there is no evident correlation with binding free energies.

Nevertheless, the evidence from other kinds of experiments can also be used in order to interpret the simulated results. Ferraresso et al. (2022) demonstrated that LNPs with ALC-0315 were better than LNPs with DLin-MC3-DMA for siRNA delivery to hepatocytes and hepatic stellate cells. Additionally, they reported the increase in markers of liver toxicity (alanine aminotransferase and bile acids) at high doses of LNPs with ALC-0315 while nothing similar was observed for the formulation with DLin-MC3-DMA. Such findings demonstrate that ALC-0315 can probably enter cell membranes easier than DLin-MC3-DMA.

In formulations with DOPE lipids DLin-MC3-DMA was not considered as a potential candidate for an optimal formulation by Ly et al. (2022) either due to low protein expression. ALC-0315 appeared to be in 2 optimized vaccine candidates, including the one with critical quality attributes, while SM-102 was considered only in one formulation. This can also be related to our observations from free energy simulations.

According to Eygeris et al. (2021), when selecting a certain ionizable lipid for delivery of various RNAs one should consider pK_a values in the range of 6–7, and for *clogP* the range 15–20 is most appropriate. From the results for binding free energies it is clear that one has to consider
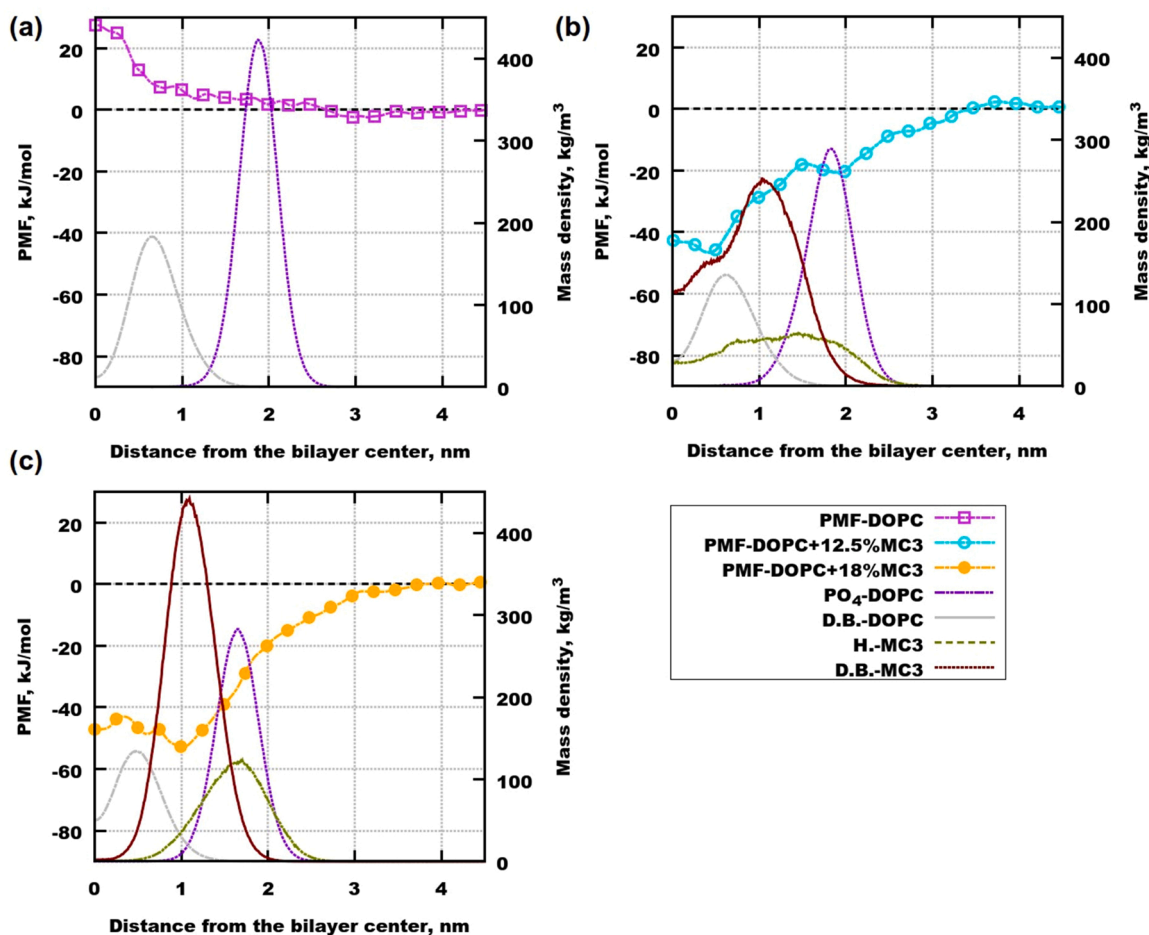
Fig. 7. Potential of mean force (PMF) and partial mass densities for systems with DOPC and DLin-MC3-DMA. (a) The system of pure DOPC. (b) The system with 12.5% of DLin-MC3-DMA. (c) The system with 18% of DLin-MC3-DMA. Partial mass densities for DLin-MC3-DMA were rescaled for clarity in (b) and (c) by factors of 8 and 10 respectively, while those densities were kept at their original values for the parts of DOPC lipids. Abbreviations on legends were the following: "PO_4-DOPC" - phosphatic groups of DOPC, "D.B.-DOPC" - double bonds of DOPC, "H.-MC3″ - head group of DLin-MC3-DMA, "D.B.-MC3″ - double bonds of DLin-MC3-DMA. The DLin-MC3-DMA molecule which was used for biasing of PMF was excluded from the mass density calculations. Errors in binding free energies are within 2 kJ/mol while in temperatures can be seen in references, mentioned above.

Table 2

pK$_a$ and *clogP* for ionizable lipids.

System	pK$_a$	clogP
DLin-MC3-DMA	6.35 Hassett et al. (2019),Suzuki and Ishihara (2021)	17.687 Eygeris et al. (2021)
ALC-0315	6.09 Ansell and Du (2015),Suzuki and Ishihara (2021)	17.198 Eygeris et al. (2021)
SM-102	6.68 Hassett et al. (2019),Suzuki and Ishihara (2021)	16.345 Eygeris et al. (2021)

also the chemistry of the phosholipids, i.e. the saturation of the lipid tails. However, DLin-MC3-DMA is rather different from the two other lipids since both tails are unsaturated and in addition there are other structural discrepancies.

The ability of ionizable lipids to penetrate biological cell membranes can be affected by the presence of proteins, sugars and other compounds. Nevertheless, in many computational works it was shown that binding free energies from *in silico* experiments could accurately predict the ability of a certain substance to penetrate through a membrane using a passive diffusion transport (Ermilova and Lyubartsev, 2017; Parisio et al., 2013; van den Berg et al., 2015; Rózsa et al., 2021; Jambeck and Lyubartsev, 2013). Therefore, the probability that SM-102 and ALC-0315 will penetrate cell membranes containing POPC is high. This fact has to be taken into account when designing LNPs with mRNA.

4. Conclusions

Free energy calculations are very important for determining whether a phenomenon can happen spontaneously at certain conditions or not. In this work we have used parallel-tempered metadynamics simulations in order to understand the ability of ionizable lipids to penetrate phospholipids bilayers when they are in their neutral forms.

It is discovered that the phospholipid phase transition temperature is the key factor which should be considered when selecting a particular helper lipid for gene-therapies. Moreover, the saturation of lipid tails has to be taken into account for both phospholipids and ionizable lipids as well as possible synergistic effects. For instance, the unsaturated DLin-MC3-DMA had an aversion to the monocomponent membrane containing DOPC, but affinity to lipid bilayers of DOPC containing some amounts of DLin-MC3-DMA.

A comparison of ALC-0315, SM-102 and DLin-MC3-DMA in simulations with the monocomponent membrane of POPC demonstrated that ALC-0315 has the highest ability to penetrate membrane due to its low free energy value, while DLin-MC3-DMA has the lowest ability as it is unable to pass through a bilayer center according to PMF profiles.

Summarizing the results it can be noted that the fact that all ionizable lipids in their neutral forms have potentials to penetrate phospholipid membranes as well as to reside on their surfaces has to be taken into account when designing modern formulations. The first consideration shall be about the efficacy of LNPs themselves. The second consideration is the possible toxicological issues as phosphatidylcholines are present in various biological cells which can lead to undesirable cytotoxicity of formulations.

When simulating ionizable lipids together with phospholipids the saturation of the latter ones has to be taken into consideration as conclusions can not be generalized for different lipid tails.

Conflicts of interest

There are no conflicts to declare.

Data Availability

Data (models) can be downloaded from Zenodo repository using the following link: https://zenodo.org/record/7794523#.ZDQ-adJBxkg .

Acknowledgement

Notes

The authors declare no competing financial interest.

Appendix A. Supporting information

Supplementary data associated with this article can be found in the online version at doi:10.1016/j.chemphyslip.2023.105294.

References

Abrams, C., Bussi, G., 2013. Enhanced sampling in molecular dynamics using metadynamics, replica-exchange, and temperature-acceleration. Entropy 16, 163–199.

Albertsen, C.H., Kulkarni, J., Witzigmann, D., Lind, M., Petersson, K., Simonsen, J.B., 2022. The role of lipid components in lipid nanoparticles for vaccines and gene therapy. Adv. Drug Deliv. Rev., 114416

Ansell, S.M., Du, X. Novel lipids and lipid nanoparticle formulations for delivery of nucleic acids.2015.

Awan, U.A., Malik, M.W., Kamran, S., Ahmed, H., Haq, M., Afzal, M.S., 2022. Wild poliovirus outbreak in Afghanistan: a wake-up call for global health experts. J. Infect. 84, 834–872.

Barducci, A., Bussi, G., Parrinello, M., 2008. Well-tempered metadynamics: a smoothly converging and tunable free-energy method. Phys. Rev. Lett. 100, 020603.

Becke, A.D., 1993. Density functional thermochemistry. III. The role of exact exchange. J. Chem. Phys. 98, 5648–5652.

Benesty, J., Chen, J., Huang, Y., Cohen, I., 2009. Noise reduction in speech processing. Springer, pp. 1–4.

Berendsen, H.J.C., Postma, J.P.M., van Gunsteren, W.F., Nola, A.D., Haak, J.R., 1984. Molecular dynamics with coupling to an external bath. J. Chem. Phys. 81, 3684–3690.

Berendsen, H.J.C., van der Spoel, D., Drunen, R., 1995. GROMACS: a message-passing parallel molecular dynamics implementation. Comp. Phys. Commun. 91, 43–56.

Bonomi, M., Barducci, A., Parrinello, M., 2009. Reconstructing the equilibrium Boltzmann distribution from well-tempered metadynamics. J. Comput. Chem. 30, 1615–1621.

Brader, M.L., Williams, S.J., Banks, J.M., Hui, W.H., Zhou, Z.H., Jin, L., 2021. Encapsulation state of messenger RNA inside lipid nanoparticles. Biophys. J. 120, 2766–2770.

Bussi, G., Laio, A., 2020. Using metadynamics to explore complex free-energy landscapes. Nat. Rev. Phys. 1–13.

Bussi, G., Gervasio, F.L., Laio, A., Parrinello, M., 2006. Free-energy landscape for β hairpin folding from combined parallel tempering and metadynamics. J. Am. Chem. Soc. 128, 13435–13441.

Bussi, G., Donadio, D., Parinello, M., 2007. Canonical sampling through velocity rescaling. J. Chem. Phys. 126, 014101.

Chu, N., Kučerka, N., Liu, Y., Tristram-Nagle, S., Nagle, J.F., 2005. Anomalous swelling of lipid bilayer stacks is caused by softening of the bending modulus. Phys. Rev. E 71, 041904.

Cornell, W.D., Cieplak, P., Bayly, C.I., Kollman, P.A., 2002. Application of RESP charges to calculate conformational energies, hydrogen bond energies, and free energies of solvation. J. Am. Chem. Soc. 115, 9620–9631.

Cui, L., Hunter, M.R., Sonzini, S., Pereira, S., Romanelli, S.M., Liu, K., Li, W., Liang, L., Yang, B., Mahmoudi, N., Desai, A.S., 2022. Mechanistic studies of an automated lipid nanoparticle reveal critical pharmaceutical properties associated with enhanced mRNA functional delivery in vitro and in vivo. Small 18, 2105832.

Darden, T., York, D., Pedersen, L., 1993. Particle mesh Ewald: an N log (N) method for Ewald sums in large systems. J. Chem. Phys. 98, 10089–10092.

Deighan, M., Bonomi, M., Pfaendtner, J., 2012. Efficient simulation of explicitly solvated proteins in the well-tempered ensemble. J. Chem. Theory Comput. 8, 2189–2192.

Dupradeau, F.-Y., Pigache, A., Zaffran, T., Savineau, C., Lelong, R., Grivel, N., Lelong, D., Rosanski, W., Cieplak, P., 2010. The REd. Tools: Advances in RESP and ESP charge derivation and force field library building. Phys. Chem. Chem. Phys. 12, 7821–7839.

Ermilova, I., Lyubartsev, A.P., 2016. Extension of the slipids force field to polyunsaturated lipids. J. Phys. Chem. B 120, 12826–12842.

Ermilova, I., Lyubartsev, A.P., 2017. Quantum chemical and molecular dynamics simulations of hydroxylated polybrominated diphenyl ethers. Phys. Chem. Chem. Phys. 19, 28263–28274.

Ermilova, I., Lyubartsev, A.P., 2019. Cholesterol in phospholipid bilayers: positions and orientations inside membranes with different unsaturation degrees. Soft Matter 15, 78–93.

Ermilova, I., Lyubartsev, A.P., 2020. Modelling of interactions between Aβ (25–35) peptide and phospholipid bilayers: effects of cholesterol and lipid saturation. RSC Adv. 10, 3902–3915.

Ermilova, I., Swenson, J., 2020. DOPC versus DOPE as a helper lipid for gene-therapies: molecular dynamics simulations with DLin-MC3-DMA. Phys. Chem. Chem. Phys. 22, 28256–28268.

Ermilova, I., Stenberg, S., Lyubartsev, A.P., 2017. Quantum chemical and molecular dynamics modelling of hydroxylated polybrominated diphenyl ethers. Phys. Chem. Chem. Phys. 19, 28263–28274.

Essmann, U., Perera, L., Berkowitz, M.L., Darden, T., Lee, H., Pedersen, L.G., 1995. A smooth particle mesh Ewald method. J. Chem. Phys. 103, 8577–8593.

Eygeris, Y., Gupta, M., Kim, J., Sahay, G., 2021. Chemistry of lipid nanoparticles for RNA delivery. Acc. Chem. Res. 55, 2–12.

Ferraresso, F., Strilchuk, A.W., Juang, L.J., Poole, L.G., Luyendyk, J.P., Kastrup, C.J., 2022. Comparison of DLin-MC3-DMA and ALC-0315 for siRNA delivery to hepatocytes and hepatic stellate cells. Mol. Pharm.

Filippov, A., Orädd, G., Lindblom, G., 2003. Influence of cholesterol and water content on phospholipid lateral diffusion in bilayers. Langmuir 19, 6397–6400.

Filippov, A., Orädd, G., Lindblom, G., 2007. Domain formation in model membranes studied by pulsed-field gradient-NMR: the role of lipid polyunsaturation. Biophys. J. 93, 3182–3190.

Frisch, M.J., Trucks, G.W., Schlegel, H.B., Scuseria, G.E., Robb, M.A., Cheeseman, J.R., Scalmani, G., Barone, V., Mennucci, B., Petersson, G.A., Nakatsuji, H., Caricato, M., Li, X., Hratchian, H.P., Izmaylov, A.F., Bloino, J., Zheng, G., Sonnenberg, J.L., Hada, M., Ehara, M., Toyota, K., Fukuda, R., Hasegawa, J., Ishida, M., Nakajima, T., Honda, Y., Kitao, O., Nakai, H., Vreven, T., Montgomery, J.A., Jr.; Peralta, J.E., Ogliaro, F., Bearpark, M., Heyd, J.J., Brothers, E., Kudin, K.N., Staroverov, V.N., Kobayashi, R., Normand, J., Raghavachari, K., Rendell, A., Burant, J.C., Iyengar, S.S., Tomasi, J., Cossi, M., Rega, N., Millam, J.M., Klene, M., Knox, J.E., Cross, J.B., Bakken, V., Adamo, C., Jaramillo, J., Gomperts, R., Stratmann, R.E., Yazyev, O., Austin, A.J., Cammi, R., Pomelli, C., Ochterski, J.W., Martin, R.L., Morokuma, K., Zakrzewski, V.G., Voth, G.A., Salvador, P., Dannenberg, J.J., Dapprich, S., Daniels, A.D., Farkas Foresman, J.B., Ortiz, J.V., Cioslowski, J., Fox, D.J. Gaussian-09 Revision D.01.2009.

Golla, V.K., Prajapati, J.D., Joshi, M., Kleinekathöofer, U., 2020. Exploration of free energy surfaces across a membrane channel using metadynamics and umbrella sampling. J. Chem. Theory Comput. 16, 2751–2765.

Grabowska-Pyrzewicz, W., Want, A., Leszek, J., Wojda, U., 2021. Antisense oligonucleotides for Alzheimeras disease therapy: from the mRNA to miRNA paradigm. EBioMedicine 74, 103691.

Gu, R.-X., Baoukina, S., Tieleman, D.P., 2019. Cholesterol flip-flop in heterogeneous membranes. J. Chem. Theory Comput. 15, 2064–2070.

Hadas, Y., Sultana, N., Youssef, E., Sharkar, M.T.K., Kaur, K., Chepurko, E., Zangi, L., 2019. Optimizing modified mRNA in vitro synthesis protocol for heart gene therapy. Mol. Ther. Methods Clin. Dev. 14, 300–305.

Hassett, K.J., Benenato, K.E., Jacquinet, E., Lee, A., Woods, A., Yuzhakov, O., Himansu, S., Deterling, J., Geilich, B.M., Ketova, T., Mihai, C., Lynn, A., McFadyen, I., Moore, M.J., Senn, J.J., Stanton, M.G., Almarsson, Ö., Ciaramella, G., Brito, L.A., 2019. Optimization of lipid nanoparticles for intramuscular administration of mRNA vaccines. Mol. Ther. Nucleic Acids 15, 1–11.

He, L., Niemeyer, B., 2003. A novel correlation for protein diffusion coefficients based on molecular weight and radius of gyration. Biotechnol. Prog. 19, 544–548.

Heberle, F.A., Petruzielo, R.S., Pan, J., Drazba, P., Kučerka, N., Standaert, R.F., Feigenson, G.W., Katsaras, J., 2013. Bilayer thickness mismatch controls domain size in model membranes. J. Am. Chem. Soc. 135, 6853–6859.

Hess, B., Bekker, H., Berendsen, H.J.C., Fraaije, J.G.E.M., 1997. LINCS: alinear constraint solver for molecular simulations. J. Comput. Chem. 18, 1463–1472.

Hess, B., 2008. P-LINCS: a parallel linear constraint solver for molecular simulation. J. Chem. Theory Comput. 4, 116–122.

Jämbeck, J.P.M., Lyubartsev, A.P., 2012. Derivation and systematic validation of a refined all-atom force field for phosphatidylcholine lipids. J. Phys. Chem. B 116, 3164–3179.

Jämbeck, J.P.M., Lyubartsev, A.P., 2013. Another piece of the membrane puzzle: extending slipids further. J. Chem. Theory Comput. 9, 774–784.

Jablin, M.S., Akabori, K., Nagle, J., 2014. Experimental support for tilt-dependent theory of biomembrane mechanics. Phys. Rev. Lett. 113, 248102.

Jambeck, J.P., Lyubartsev, A.P., 2013. Exploring the free energy landscape of solutes embedded in lipid bilayers. J. Phys. Chem. Lett. 4, 1781–1787.

Jayaraman, M., Ansell, S.M., Mui, B.L., Tam, Y.K., Chen, J., Du, X., Butler, D., Eltepu, L., Matsuda, S., Narayanannair, J.K., Rajeev, K., Hafez, I.M., Akinc, A., Maier, M.A., Tracy, M.A., Cullis, P.R., Maden, T.D., Manoharan, M., Hope, M.J., 2012. Maximizing the potency of siRNA lipid nanoparticles for hepatic gene silencing in vivo. Ang. Chem. Int. Ed. 51, 8529–8533.

Jorgensen, W.L., Chandrasekhar, J., Madura, J.D., Impey, R.W., Klein, M.L., 1983. Comparison of simple potential functions for simulating liquid water. J. Chem. Phys. 79, 926–935.

Kendall, R.A., Dunning Jr, T.H., Harrison, R.J., 1992. Electron affinities of the first-row atoms revisited. Systematic basis sets and wave functions. J. Chem. Phys. 96, 6796–6806.

Kon, E., Elia, U., Peer, D., 2022. Principles for designing an optimal mRNA lipid nanoparticle vaccine. Curr. Opin. Biotechnol. 73, 329–336.

Kucherak, O.A., Oncul, S., Darwich, Z., Yushchenko, D.A., Arntz, Y., Didier, P., Mély, Y., Klymchenko, A.S., 2010. Switchable nile red-based probe for cholesterol and lipid order at the outer leaflet of biomembranes. J. Am. Chem. Soc. 132, 4907–4916.

Kulkarni, J.A., Myhre, J.L., Chen, S., Tam, Y.Y.C., Danescu, A., Richman, J.M., Cullis, P.R., 2017. Design of lipid nanoparticles for in vitro and in vivo delivery of plasmid DNA. Nanomed.: Nanotech., Biol. Med. 13, 1377–1387.

Kulkarni, J.A., Witzigmann, D., Leung, J., Tam, Y.Y.C., Cullis, P.R., 2019. On the role of helper lipids in lipid nanoparticle formulations of siRNA. Nanoscale 11, 21733–21739.

Lee, C., Yang, W., Parr, R., 1988. Development of the Colle-Salvetti correlation-energy formula into a functional of the electron density. Phys. Rev. B 37, 785. AD Becke, Density-Functional Thermochemistry. III. The Role of Exact Exchange. J. Chem. Phys 1993, 98, 5648.

Lei, S., Zhang, X., Li, J., Gao, Y., Wu, J., Duan, X., Men, K., 2020. Current progress in messenger RNA-based gene therapy. J. Biomed. Nanotech. 16, 1018–1044.

Lindblom, G., Orädd, G., 2009. Lipid lateral diffusion and membrane heterogeneity. Biochim. Biophys. BBA 1788, 234–244.

Lobanov, M.Y., Bogatyreva, N., Galzitskaya, O., 2008. Radius of gyration as an indicator of protein structure compactness. Mol. Biol. 42, 623–628.

Ly, H.H., Daniel, S., Soriano, S.K., Kis, Z., Blakney, A.K., 2022. Optimization of lipid nanoparticles for saRNA expression and cellular activation using a design-of-experiment approach. Mol. Pharm.

Makoni, M., 2022. Ebola outbreak in DR Congo. Lancet 399, 1766.

Malburet, C., Leclercq, L., Cotte, J.-F., Thiebaud, J., Bazin, E., Garinot, M., Cottet, H., 2022. Size and charge characterization of lipid nanoparticles for mRNA vaccines. Anal. Chem. 94, 4677–4685.

Martí, J., 2018. Free-energy surfaces of ionic adsorption in cholesterol-free and cholesterol-rich phospholipid membranes. Mol. Simul. 44, 1136–1146.

May, S., Kozlovsky, Y., Ben-Shaul, A., Kozlov, M., 2004. Tilt modulus of a lipid monolayer. Eur. Phys. J. E 14, 299–308.

Munson, M.J., O'Driscoll, G., Silva, A.M., Lázaro-Ibáñez, E., Gallud, A., Wilson, J.T., Collén, A., Esbjörner, E.K., Sabirsh, A., 2021. A high-throughput Galectin-9 imaging assay for quantifying nanoparticle uptake, endosomal escape and functional RNA delivery. Commun. Biol. 4, 1–14.

Nagle, J.F., Jablin, M.S., Tristram-Nagle, S., Akabori, K., 2015. What are the true values of the bending modulus of simple lipid bilayers? Chem. Phys. Lipids 185, 3–10.

Nagle, J.F., 2017. Experimentally determined tilt and bending moduli of single-component lipid bilayers. Chem. Phys. Lipids 205, 18–24.

Ndeupen, S., Qin, Z., Jacobsen, S., Bouteau, A., Estanbouli, H., Igyártó, B.Z., 2021. The mRNA-LNP platforms lipid nanoparticle component used in preclinical vaccine studies is highly inflammatory. iScience 24, 103479.

Niu, Y., Xu, F., 2020. Deciphering the power of isolation in controlling COVID-19 outbreaks. Lancet Glob. Health 8, e452–e453.

Okonji, O.C., Okonji, E.F., Mohanan, P., Babar, M.S., Saleem, A., Khawaja, U.A., Essar, M.Y., Hasan, M.M., 2022. Marburg virus disease outbreak amidst COVID-19 in the Republic of Guinea: a point of contention for the fragile health system? Clin. Epidemiol. Glob. Health 13, 100920.

Orädd, G., Lindblom, G., Westerman, P.W., 2002. Lateral diffusion of cholesterol and dimyristoylphosphatidylcholine in a lipid bilayer measured by pulsed field gradient NMR spectroscopy. Biophys. J. 83, 2702–2704.

Parisio, G., Stocchero, M., Ferrarini, A., 2013. Passive membrane permeability: beyond the standard solubility-diffusion model. J. Chem. Theory Comput. 9, 5236–5246.

Park, S., Choi, Y.K., Kim, S., Lee, J., Im, W., 2021. CHARMM-GUI membrane builder for lipid nanoparticles with ionizable cationic lipids and PEGylated lipids. J. Chem. Inf. Model. 61, 5192–5202.

Pascolo, S., 2008. Vaccination with messenger RNA (mRNA). Toll- Recept. (TLRs) innate Immun. 221–235.

Patel, S.K., Billingsley, M.M., Frazee, C., Han, X., Swingle, K.L., Qin, J., Alameh, M.-G., Wang, K., Weissman, D., Mitchell, M.J., 2022. Hydroxycholesterol substitution in ionizable lipid nanoparticles for mRNA delivery to T cells. J. Control. Release 347, 521–532.

Pfaendtner, J., 2019. Biomolecular Simulations. Springer, pp. 179–200.

Pokhrel, N., Maibaum, L., 2018. Free energy calculations of membrane permeation: challenges due to strong headgroup–solute interactions. J. Chem. Theory Comput. 14, 1762–1771.

Pomelli, C.S., Tomasi, J., Barone, V., 2001. An improved iterative solution to solve the electrostatic problem in the polarizable continuum model. Theor. Chem. Acc. 105, 446–451.

Rózsa, Z.B., Szőri-Doroghàzi, E., Viskolcz, B., Szőri, M., 2021. Transmembrane penetration mechanism of cyclic pollutants inspected by molecular dynamics and metadynamics: the case of morpholine, phenol, 1, 4-dioxane and oxane. Phys. Chem. Chem. Phys. 23, 15338–15351.

Rabinovich, P.M., Komarovskaya, M.E., Ye, Z.-J., Imai, C., Campana, D., Bahceci, E., Weissman, S.M., 2006. Synthetic messenger RNA as a tool for gene therapy. Hum. Gene Ther. 17, 1027–1035.

Söderberg, M., Edlund, C., Kristensson, K., Dallner, G., 1990. Lipid compositions of different regions of the human brain during aging. J. Neurochem. 54, 415–423.

Sahu, S., Lynn, W.S., 1977. Lipid composition of human alveolar macrophages. Inflammation 2, 83–91.

Sayers, E., Peel, S., Schantz, A., England, R., Beano, M., Bates, S., Desai, A., Puri, S., Ashford, M., Jones, A., 2019. Endocytic profiling of cancer cell models reveals critical factors influencing lipid nanoparticle mediated mRNA delivery and protein expression. Mol. Ther. 27.

Schoenmaker, L., Witzigmann, D., Kulkarni, J.A., Verbeke, R., Kersten, G., Jiskoot, W., Crommelin, D.J., 2021. mRNA-lipid nanoparticle COVID-19 vaccines: structure and stability. Int. J. Pharm. 601, 120586.

Sebastiani, F., YanezArteta, M., Lerche, M., Porcar, L., Lang, C., Bragg, R.A., Elmore, C.S., Krishnamurthy, V.R., Russell, R.A., Darwish, T., Pichler, H., Waldie, S., Moulin, M., Haertlein, M., Forsyth, T.V., Lindfors, L., Cardenás, M., 2021. Apolipoprotein E binding drives structural and compositional rearrangement of mRNA-containing lipid nanoparticles. ACS nano 15, 6709–6722.

Sedgwick, P., 2012. Pearsonas correlation coefficient. Bmj 345.

Silvius, J.R., 1982. Thermotropic phase transitions of pure lipids in model membranes and their modifications by membrane proteins. Lipid-Prot. Interact. 2, 239–281.

Silvius, J.R., 1991. Thermotropic properties of phospholipid analogues. Chem. Phys. Lipids 57, 241–252.

Stephens, P.J., Devlin, F., Chabalowski, C., 1994. M. J. Ab initio calculation of vibrational absorption and circular dichroism spectra using density functional force fields. J. Phys. Chem. Lett. 98, 11623–11627.

Suzuki, Y., Ishihara, H., 2021. Difference in the lipid nanoparticle technology employed in three approved siRNA (Patisiran) and mRNA (COVID-19 vaccine) drugs. Drug Metab. Pharmacokinet. 41, 100424.

Szlasa, W., Zendran, I., Zalesińska, A., Tarek, M., Kulbacka, J., 2020. Lipid composition of the cancer cell membrane. J. Bioenerg. Biomembr. 52, 321–342.

Tomasi, J., Mennucci, B., Cances, E., 1999. The IEF version of the PCM solvation method: an overview of a new method addressed to study molecular solutes at the QM ab initio level. THEOCHEM 464, 211–226.

Tribello, G.A., Bonomi, M., Branduardi, D., Camilloni, C., Bussi, G., 2014. PLUMED 2: new feathers for an old bird. Comput. Phys. Comm. 185, 604–613.

Tristram-Nagle, S., Petrache, H.I., Nagle, J.F., 1998. Structure and interactions of fully hydrated dioleoylphosphatidylcholine bilayers. Biophys. J. 75, 917–925.

van den Berg, B., PrathyushaBhamidimarri, S., DahyabhaiPrajapati, J., Kleinekathöfer, U., Winterhalter, M., 2015. Outer-membrane translocation of bulky small molecules by passive diffusion. Proc. Natl. Acad. Sci. 112, E2991–E2999.

Venkatesan, P., 2022. Global monkeypox outbreak. Lancet Infect. Dis. 22, 950.

Verbeke, R., Lentacker, I., De Smedt, S.C., Dewitte, H., 2021. The dawn of mRNA vaccines: the COVID-19 case. J. Control. Release 333, 511–520.

Viger-Gravel, J., Schantz, A., Pinon, A.C., Rossini, A.J., Schantz, S., Emsley, L., 2018. Structure of lipid nanoparticles containing siRNA or mRNA by dynamic nuclear polarization-enhanced NMR spectroscopy. J. Phys. Chem. B 122, 2073–2081.

Walter, A., Gutknecht, J., 1986. Permeability of small nonelectrolytes through lipid bilayer membranes. J. Membr. Biol. 90, 207–217.

Wang, Y., Zhang, R., Tang, L., Yang, L., 2022. Nonviral delivery systems of mRNA vaccines for cancer gene therapy. Pharmaceutics 14, 512.

Ward, D., Gomes, A.R., Tetteh, K.K., Sepúlveda, N., Gomez, L.F., Campino, S., Clark, T.G., 2022. Sero-epidemiological study of arbovirus infection following the 2015–2016 Zika virus outbreak in Cabo Verde. Sci. Rep. 12, 1–8.

Xia, X., 2021. Detailed dissection and critical evaluation of the Pfizer/BioNTech and moderna mRNA vaccines. Vaccines 9, 734.

Yanez Arteta, M., Kjellman, T., Bartesaghi, S., Wallin, S., Wu, X., Kvist, A.J., Dabkowska, A., Székely, N., Radulescu, A., Bergenholtz, J., Lindfors, L., 2018. Successful reprogramming of cellular protein production through mRNA delivered by functionalized lipid nanoparticles. Proc. Natl. Acad. Sci. 115, E3351–E3360.

Yang, J., Bonomi, M., Calero, C., Martí, J., 2016. Free energy landscapes of sodium ions bound to dmpc–cholesterol membrane surfaces at infinite dilution. Phys. Chem. Chem. Phys. 18, 9036–9041.